5   HARNESSING THE PURSE STRING FOR ACCELERATED WOUND CLOSURE

Abstract

Wound healing is essential in maintaining tissue integrity. Wounds can close via lamellipodial crawling, which involves the rapid migration of cell sheets. A slower mechanism also exists, which involves the assembly of an actomyosin cable and subsequent contraction in a "purse string" manner to close the wound. Here we vary wound geometry to generate conditions where both mechanisms act synergistically to accelerate wound closure. In wounds that take the shape of zigzag patterns, cells at the apical points develop into leader cells while the cell sheet undergoes purse string contraction in concave regions. Especially strong purse string contraction was observed in 45° zigzag wounds, resulting in nearly eight-fold faster wound healing rates compared to wounds with straight edges.

5.1   Introduction

The process of collective migration has been well-studied for its importance in wound healing, morphogenesis, and tumor metastasis. In tissue repair, wound closure can occur via two distinct mechanisms (*1*). Using cell-ECM interactions, cells at the wound edge can actively extend their lamellipodia as they migrate into the wound area (*2-3*). These leader cells guide the cells behind them, forming "finger-like" protrusions. Wound closure can also occur via a "purse string" mechanism using a continuous actomyosin cable that develops along the periphery of the wound (*4-5*). As the cable contracts, the mechanical force it generates can be transmitted through intercellular adhesions along the wound edge (*6-8*).

There are numerous strategies to influence cell migration, which include controlling surface adhesiveness (*9*), substrate stiffness (*10*), and micropatterning (*11*). We present here a novel strategy to influence cell sheet migration in wound healing in the absence of ECM. We pre-dispose wounds to a zigzag geometry and create conditions where both the lamellipodial crawling and purse string mechanisms can act synergistically to accelerate wound closure.

Although the selection of wound healing mechanism has been reported to be independent of wound shape (*12*), we report here configurations that strongly bias the selection of wound healing mechanisms based on local geometry. Whitesides and coworkers demonstrate that cells confined to a square shape are likely to form lamellipodia at corners (*13*). Likewise, in zigzag wounds, cells located at the apex have a high propensity to develop into leader cells. Conversely, cells confined to concave

regions are likely to undergo purse string contractions. Local geometry at the apex induced the formation of leader cells, but on glass surfaces, cells were unable to migrate into the wound area. The traction forces generated by the leader cells however, generate tension in the adjacent actomyosin cables. The tension reinforces purse string contraction in the neighboring regions and drives the cell sheet forward. We further hypothesize that the propensity for leader cell formation increases with decreasing angle θ at the apex, and that the resulting contractile forces will increase with decreasing angle (Figure 5.1).
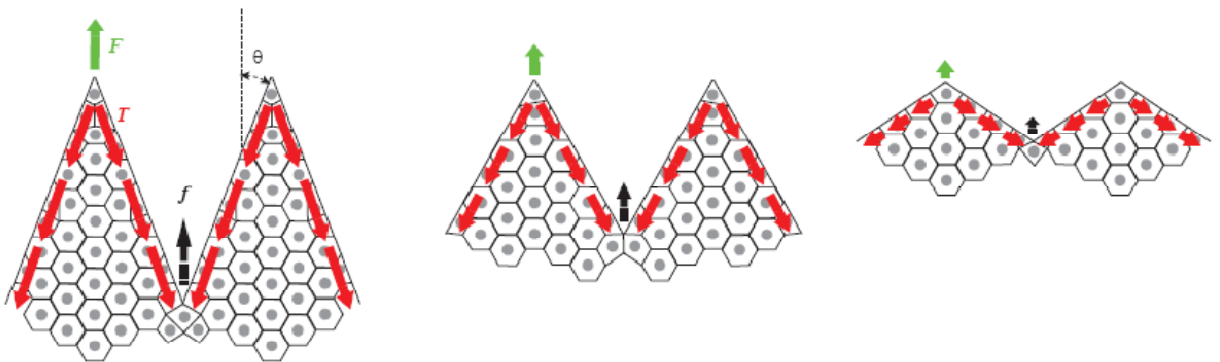

Figure 5.1 Schematic of wound closure in zigzag wounds and the effect of angles on purse string contraction. Cells at the apex develop into leader cells and create traction forces (F, green arrows) that are transmitted through the neighboring actomyosin cables (red arrows). The increased tension, T strengthens the contraction forces (f, black arrows) in the actomyosin purse string, drawing the cell sheet forward. The propensity for leader cell formation increases with decreasing angle θ at the apex, and contraction forces are expected to increase with decreasing angle.

5.2   Materials and methods

Cell culture

Madin-Darby Canine Kidney (MDCK) cells were cultured in Dulbecco's modified eagle medium (DMEM) containing 10% fetal bovine serum, 1% penicillin/streptomycin, and phenol-red (growth medium). All experiments were performed in DMEM lacking phenol-red, supplemented with 1% penicillin/streptomycin (serum-free medium).

Wound healing with micropatterned PDMS blocks

The micropatterned PDMS blocks were fabricated as described in Chapter 4. The wound features were designed using DesignCAD software and printed on transparencies as positive photomasks (CAD/Art Services, Inc., Bandon, OR) as shown in Figure 5.2A. Similarly, the wound healing assay used in this work was described in Chapter 4 (Figure 5.2A).

Fluorescence imaging

The MDCK cell monolayers were wounded and maintained in serum-free media at 37 ºC for 4 h. Cells were fixed with pre-warmed 3.7% paraformaldehyde in PBS at pH 7.5 for 20 min at 37 ºC. After washing with PBS, cells were blocked in blocking solution (10% FCS, 5% sucrose, 2% BSA in PBS) for 30 min at room temperature. To visualize actin, cells were incubated with phalloidin-rhodamine (1:50 in PBS, Molecular Probes, Inc., Eugene, OR) for 1 h 37 ºC. Glass coverslips were mounted with 1:1 glycerol in PBS

and imaged using an Zeiss Axiovert 200 M microscope with epifluorescence optics and AxioVision LE software.

Data analysis

The wound areas demarcated by the red box (Figure 5.3B) were traced manually using ImageJ v1.42 (NIH). The displacement of the cell sheet in the direction of the wound was calculated by dividing the change in the wound area by the length of the wound (l) at various time points. The point on the wound edge furthest from the apex was followed for 24 h using MTrackJ, an ImageJ plugin developed by Meijering and coworkers at the Biomedical Imaging Group Rotterdam. The displacement was averaged for all videos and plotted as a function of time for each angle. The data was fitted to a linear fit and the slopes resulting from the fit were reported as contractile speeds (μm/h).

Statistical Analysis

For all experimental data, the statistical significance of differences was estimated by analysis of variance followed by the Tukey test. Differences were taken to be significant at $P \leq 0.05$.

5.3   Results and discussion

As expected, the zigzag wound geometry promoted both leader cells and actomyosin purse strings at the apex and concave regions, respectively. After 4 h, cells developed lamellipodia in convex regions (indicated by position b in Figure 5.2A), which were similar to "finger-like" leader cell protrusions (*3*). As expected, the purse string mechanism was dominant in concave regions of the wound edge (position c in Figure 5.2A). Images of the wound edge labeled with F-actin confirmed the presence of lamellipodia and actomyosin purse string cables in these regions (Figures 5.2B and C).
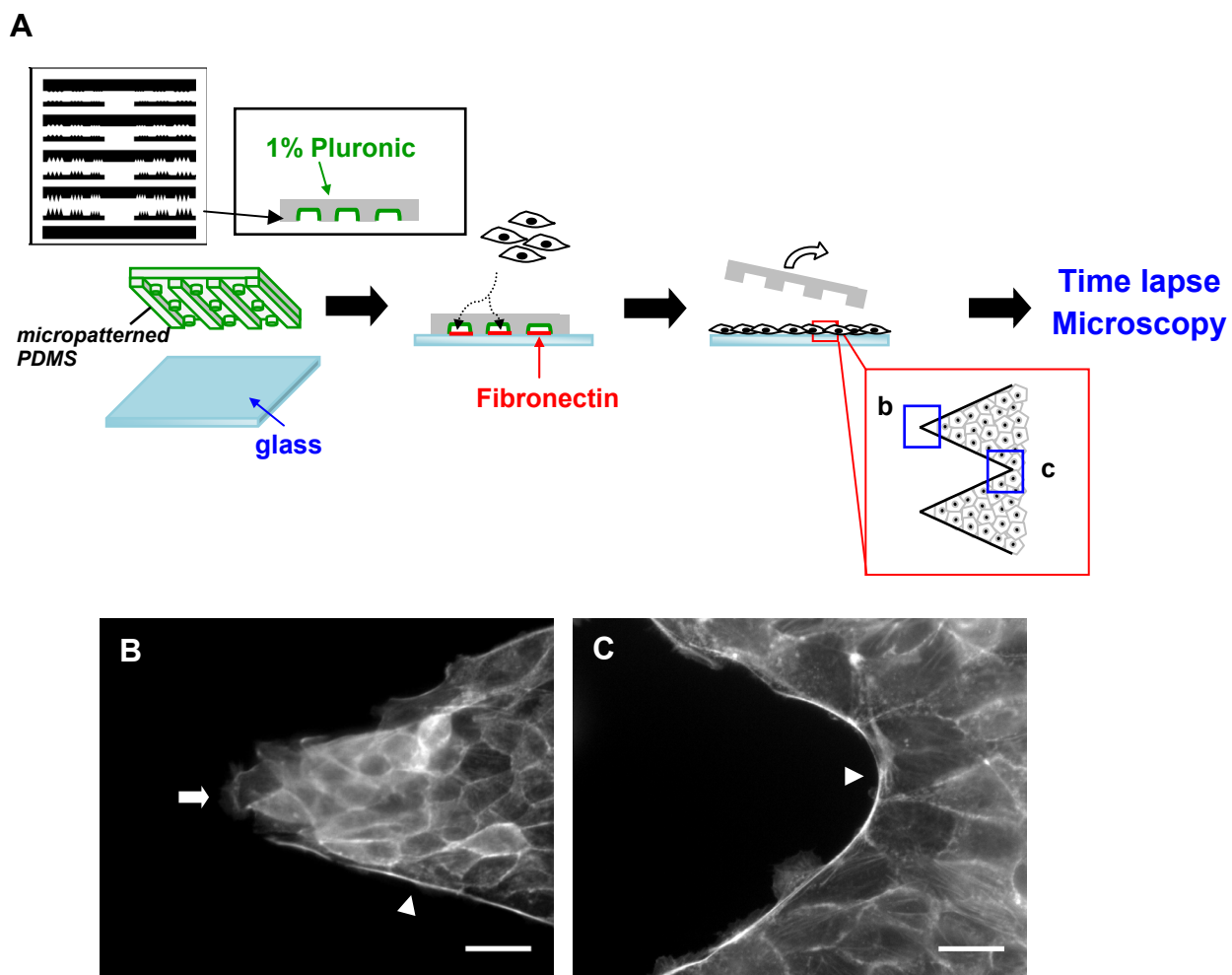
Figure 5.2 Initial wound geometry determines mode of wound healing. (**A**) Schematic of wound healing assay. The PDMS micropatterns were released and MDCK cell monolayers were allowed to migrate on glass surfaces for 4 h in serum-free media. Cells were fixed and stained with phalloidin-rhodamine. (**B, C**) Fluorescence images show the formation of leader cells (white arrow) and purse string structures (white triangles) after 4 h, corresponding to positions b and c as shown in **A**. Scale bars represent 20 µm.

Figure 5.3A shows time-lapse images of zigzag wounds for varying angles 2θ. For all zigzag wounds with $2\theta = 45°$, cells in the convex regions extended their lamellipodia, but did not migrate into the wound area. Instead, cells often rearranged themselves at the corners while preserving the "finger-like" patterns. In the concave regions of the cell sheet, purse strings contracted in the direction of the wound, propelling the cell sheet forward. At later times (> 20 h), the finger-like patterns also became motile. Wounds with $2\theta = 45°$ are most likely to promote the formation of leader cells.

Similar behavior was also observed in zigzag wounds with larger angles. Although cells at the apex extend lamellipodia, these finger-like features were quickly re-integrated into the cell sheet. Nonetheless, purse string contractions were also observed in the concave regions, giving rise to net movement in the direction of the wound. In comparison, minimal migration was observed on the straight-edged wounds (i.e., $2\theta = 180°$).

To quantify the wound closure rates, we manually tracked the change in the wound area over time (Figure 5.3B). We represented the displacement of the cell sheet by dividing the change in the wound area by the length of the cell sheet, l (Figure 5.3C). The wound closure rates were obtained by fitting the data from time interval t = 12 h to 22 h to a linear fit (Table 5.1).
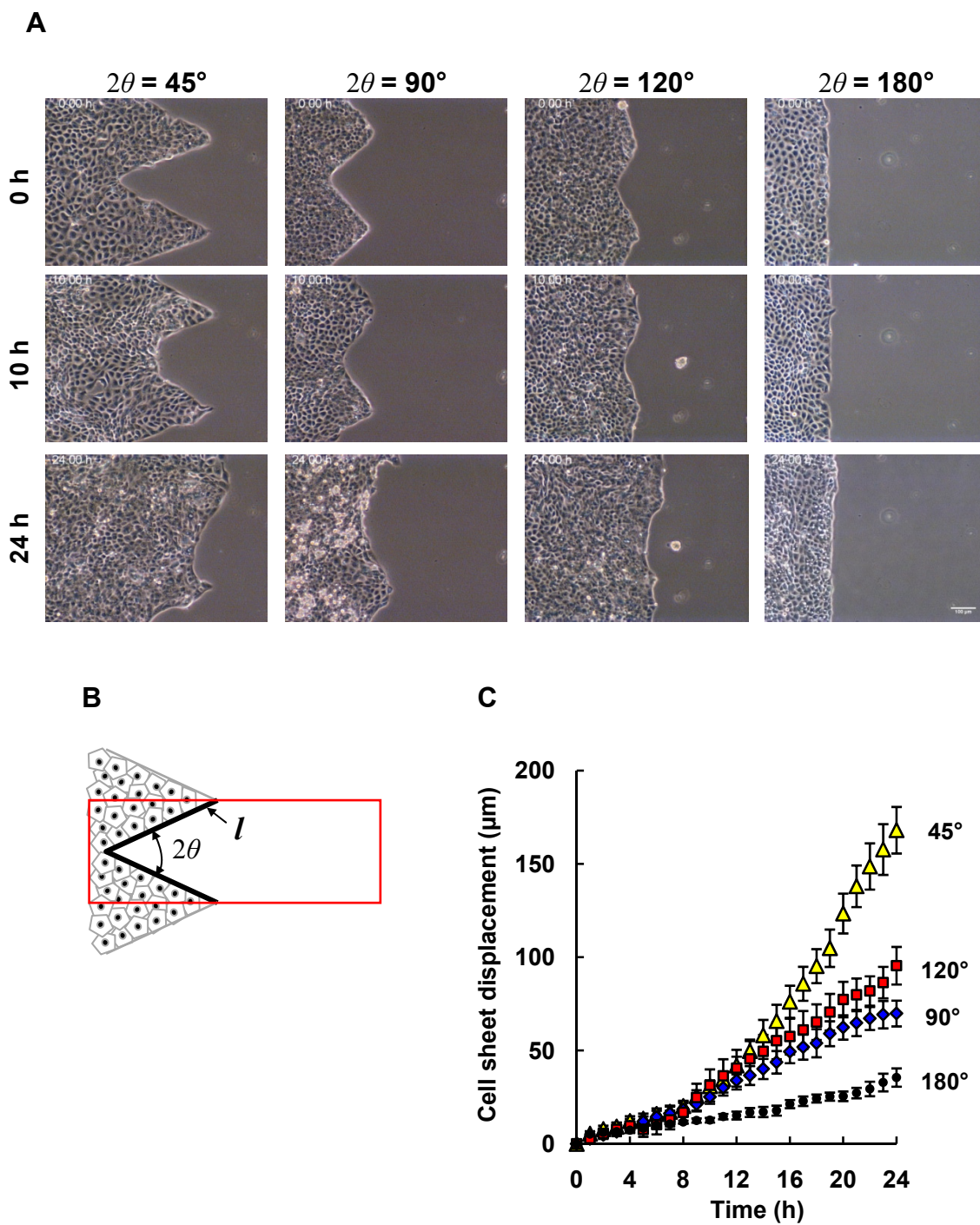
A

B

C

Figure 5.3 Time course of wound healing for zigzag wounds. (**A**) Time-lapse images of various zigzag wounds with angles 2θ. Scale bar represents 100 μm for all images. (**B**) Schematic of the wound closure analysis. The length of the wound (l) is highlighted in black. (**C**) The displacement of the cell sheet over time. Cell sheet displacement for each time point was

calculated by measuring the change in wound area within the red box and divided by the length of the wound (l). Data are means ± SEM for at least 10 independent experiments.

2θ	Wound closure rate ± S.E. (µm/h) $t = 12$ to 22 h
45	10.7 ± 0.5
90	3.5 ± 0.1
120	4.2 ± 0.1
180	1.4 ± 0.1

Table 5.1 Wound closure rates as a function of 2θ. The data in Figure 5.3C were subjected to linear fits for time intervals $t = 12$ to 22 h. The slopes obtained from the fit are reported as wound closure rates ± S.E.

The overall wound closure rates for zigzag wounds with $2\theta = 45°$ was 7.6-fold higher than for a straight-edged wound ($2\theta = 180°$) (Table 5.1). These wounds promoted rapid contraction of the wound edge via the actomyosin purse string with speeds up to 20 µm/h (Figure 5.4). In comparison, contractile speeds for purse strings resulting from zigzag wounds with larger angles were two-fold lower (Figure 5.4).
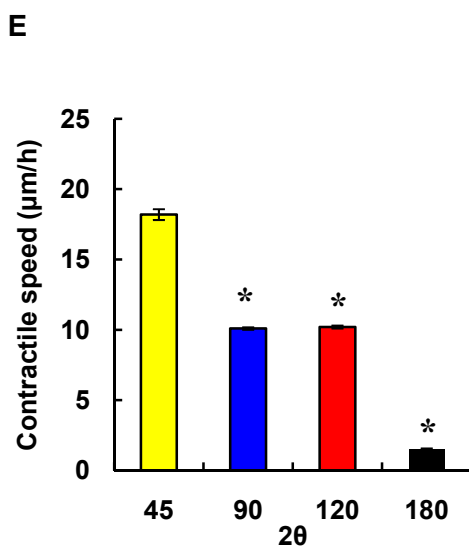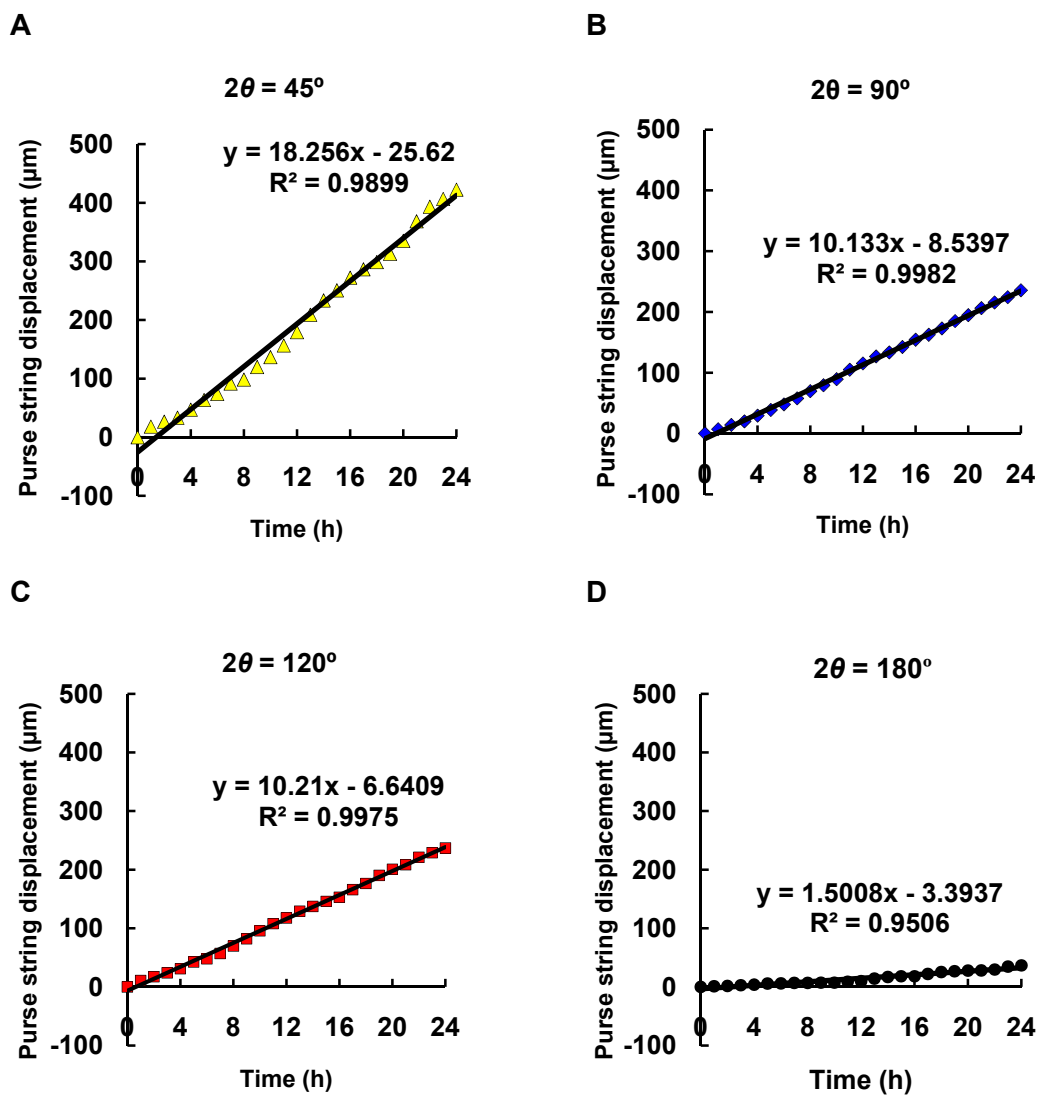
A $2\theta = 45^\circ$

y = 18.256x - 25.62
R² = 0.9899

B $2\theta = 90^\circ$

y = 10.133x - 8.5397
R² = 0.9982

C $2\theta = 120^\circ$

y = 10.21x - 6.6409
R² = 0.9975

D $2\theta = 180^\circ$

y = 1.5008x - 3.3937
R² = 0.9506

E

Figure 5.4 Overall contractile speed of purse string as a function of 2θ. The point on the wound edge furthest away from the apex was tracked manually for 24 h and the displacement of the purse string was measured over time. (**A** to **D**) Average purse string displacement over time of all the videos analyzed. (**E**) Contractile speed of purse string for zigzag wounds of with angles 2θ. Data are slopes from fitted data shown in **A** to **D**. Error bars are standard errors calculated from the fit. *, significant difference from 2θ = 45°.

5.4   Conclusions

In summary, we demonstrate the synergistic use of both wound healing modes to accelerate wound closure. We also demonstrate that cells at the wound edge can be made to adopt specific wound healing mechanisms based on the local geometry. By patterning wound geometry in a zigzag shape, we show that cells at the apex develop into leader cells and cells at concave regions activate the actomyosin purse string. Under these conditions, leader cells generate traction forces that are transmitted through the actomyosin purse strings. The increased tension results in higher contractile forces, pulling the cell sheet forward. As a result of the strengthened purse string contraction, wound closure rates were increased nearly eight-fold in zigzag wounds with the smallest angles (i.e. 2θ = 45°), compared to wounds with straight edges.

5.5 Acknowledgements

5.6 References

1.   P. Martin, J. Lewis, *Nat. Lett.* **360**, 179 (1992).

2.   G. Fenteany, P. A. Janmey, T. P. Stossel, *Curr. Biol.* **10**, 831 (2000).

3.   T. Omelchenko, J. M. Vasiliev, I. M. Gelfand, H. H. Feder, E. M. Bonder, *Proc. Natl. Acad. Sci. USA* **100**, 10788 (2003).

4.   W. M. Bement, P. Forscher, M. S. Mooseker, *J. Cell Biol.* **121**, 565 (1993).

5.   D. P. Kiehart, *Curr. Biol.* **9**, R602 (1999).

6.   M. Tamada, T. D. Perez, W. J. Nelson, M. P. Sheetz, *J. Cell Biol.* **176**, 27 (2007).

7.   Y. Danjo, I. K. Gipson, *J. Cell Sci.* **111**, 3323 (1998).

8.   O. M. Rossier et al., *EMBO J.* **29**, 1055 (2010).

9.   S. P. Palecek, J. C. Loftus, M. H. Ginsberg, D. A. Lauffenburger, *Nature* **385**, 537 (1997).

10. C. M. Lo, H. B. Wang, M. Dembo, Y-L. Wang, *Biophys. J.* **79**, 144 (2000).

11. X. Jiang, D. A. Bruzewicz., A. P. Wong, M. Piel, G. M. Whitesides, *Proc. Natl. Acad. Sci. USA* **102**, 975 (2005).

12. S. Grasso, J. A. Hernandez, S. Chifflet, *Am. J. Physiol. Cell Physiol.* **293**, C1327 (2007).

13. K. K. Parker et al., *FASEB J.* **16**, 1195 (2002).